

**Manuscript presented at the 5th International Conference on Information Processing in Computer-Assisted Interventions, and published in Lecture Notes in Computer Science, vol. 8498, pp. 246-255, 2014.
DOI:10.1007/978-3-319-07521-1_26.**

The final version of the paper is available at:

http://link.springer.com/chapter/10.1007/978-3-319-07521-1_26

2D/3D Catheter-based Registration for Image Guidance in TACE of Liver Tumors

Pierre Ambrosini¹, Danny Ruijters², Adriaan Moelker³, Wiro J. Niessen^{1,4},
and Theo van Walsum¹

¹ Biomedical Imaging Group Rotterdam,
Department of Radiology and Medical Informatics,
Erasmus MC, Rotterdam, The Netherlands

p.ambrosini@erasmusmc.nl

² Philips Healthcare, Interventional X-ray Innovation, Best, The Netherlands

³ Department of Radiology, Erasmus MC, Rotterdam, The Netherlands

⁴ Imaging Science and Technology, Faculty of Applied Sciences,
Delft University of Technology, Delft, The Netherlands

Abstract. Image fusion of liver 2D X-ray images and pre or peri-operative 3D reconstructions can add valuable contextual information during image guided interventions. Such image fusion requires 2D/3D registration. In abdominal interventions, such as TACE of liver tumors, the initial alignment may be invalidated by e.g. breathing motion. We present a method that maintains the alignment between 3D Rotational Angiography (3DRA) and 2D X-ray, using the catheter position. To this end, we use the catheter in the 2D X-ray and the blood vessels in the 3DRA, then fuse 2D/3D using the knowledge that the catheter is inside the vessels. The registration is performed in two steps: First, we use a shape constraint to determine the most likely catheter positions inside the blood vessel tree. Next, we perform a rigid registration and take the best transformation over all previous selected catheter positions. The method is evaluated on phantom, clinical and simulated data.

Keywords: 2D/3D, Rigid, Catheter, Registration, Guidance, X-ray, Fluoroscopy, 3DRA, Abdominal, TACE, Liver, Breathing, Compensation

1 Introduction

Minimally invasive procedures are more and more common in medical intervention. They enable procedures with minimal trauma for the patient. Image guidance is essential for minimally invasive procedures. However, common interventional modalities, such as intra-operative 2D X-ray imaging and 2D/3D ultrasound have limitations: X-ray imaging using ionizing radiation is a projection technique, and requires contrast agent to visualize vasculature. Ultrasound imaging is operator-dependent, and hard to interpret. Integration of information from 3D (pre or peri-operative) modalities to improve the image guidance may therefore be a useful strategy in minimally invasive interventions. This requires fusion of the intra-operative images with the pre or peri-operative images,

which is often performed using image registration. After an initial alignment of the 3D image to the interventional situation, patient motion or breathing may invalidate the alignment. The purpose of our work is to develop and evaluate a method to maintain this alignment in TACE procedures.

Transcatheter Arterial ChemoEmbolization (TACE) is a minimal invasive procedure to treat liver cancer (mostly Hepatocellular Carcinoma). In these procedures, a catheter is navigated towards a tumor via the femoral and hepatic artery, after which chemotherapeutic agents are injected. Currently, the interventionist guides the catheter using single plane 2D X-ray (fluoroscopy), mainly visualizing only the catheter (Fig. 1). Frequently, angiographies (2D X-ray imaging with contrast agent injection) are acquired to visualize the arteries. CTA is used pre-operatively to visualize the tumors and feedings arteries. The navigation of the catheter using only 2D fluoroscopy is hampered by the inability to continuously visualize the arterial tree.

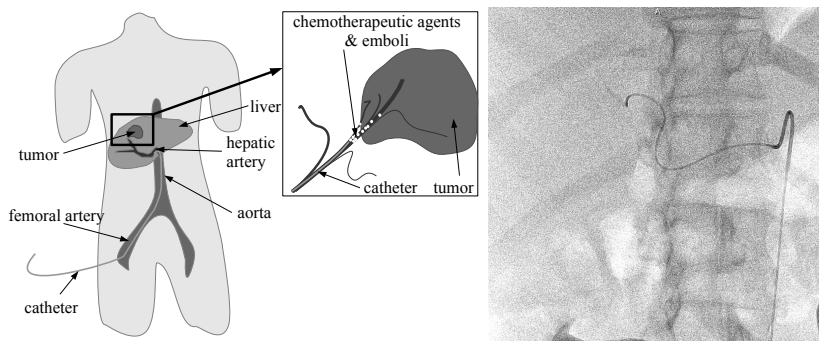


Fig. 1. (left) TACE overview. (right) Fluoroscopy example.

Fusion of the tumor and arterial tree from CTA (or from 3DRA) may greatly facilitate the navigation of the catheter to the tumor. There have been many reports on 2D/3D registration approaches to integrate 3D information in X-ray guided interventions. These approaches were described for example for abdominal [1–3], cardiac [4, 5] and neuro-vascular [6] cases (see [7, 8] for a thorough review). Most methods proposed for abdominal applications perform 2D/3D registration with single plane or bi-plane 2D intra-operative angiography and 3D pre-operative CTA [1–3]. [9] developed a semi-automatic respiratory motion tracking method using a small part of the catheter. In [6, 9], peri-operative 3DRA was used instead of pre-operative CTA, to register with 2D X-ray images using the calibrated geometry of the C-arm. Thus, the initial alignment is accurate and based only on the C-arm position, which is known.

Our method is also based on this initial alignment. However in abdominal intervention, breathing, patient and table motion lead to misalignments. We propose a novel approach for maintaining the registration and thus a spatially aligned roadmap. Such an approach may facilitate catheter navigation and re-

duce contrast agent use during intervention. Unlike most methods, 2D angiographies are not required and registration is performed for each frame independently and fully automatically. Our method uses the centerlines of the arterial tree that are extracted from a 3DRA image (acquired at the start of the intervention), and the complete catheter shape/position from the single plane fluoroscopic images. The registration uses the projection of the 3D blood vessel tree with the extracted 2D catheter shape (Fig. 2). In this work, we focus on keeping the 2D/3D alignment up-to-date. Both the arterial tree extraction (which is relatively easy given the high contrast in the 3DRA), and the real-time catheter detection, which may still be challenging [10] are not discussed here.

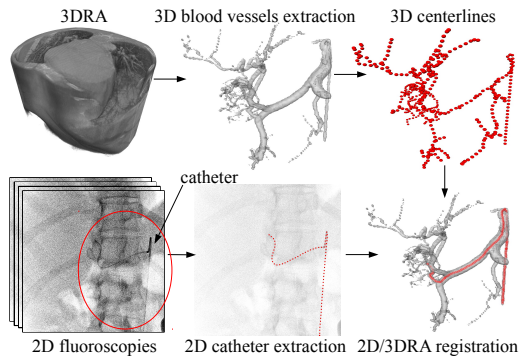


Fig. 2. Global overview

2 Methods

The registration method consists of two stages. The first stage uses a shape constraint to rank the potential vessels in the blood vessel tree to locate the most likely position of the catheter. The second stage aligns the catheter in 2D with the potential vessels that result from the previous stage. In the following, we give definitions, followed by the details of each stage.

2.1 Definitions

We define the following coordinate systems (CS) for our setup in the intervention room:

- CS_w , the world 3D CS, located at the iso-center of the C-arm, and oriented along the C-arm in its default position
- CS_{detector} , the detector 3D CS (X-ray image plane)
- CS_{fluoro} , is the 2D CS of the fluoroscopic image
- CS_{3DRA} , 3D CS of the 3DRA

Accordingly, the following coordinate transforms are defined:

- $T_{\text{detector} \leftarrow w}$, transform matrix from the world 3D CS to the detector 3D CS
- T_{proj} , cone-beam projection matrix from CS_{detector} to CS_{fluoro}
- $T_{w \leftarrow 3\text{DRA}}$, transform matrix from the 3DRA 3D CS to the world 3D CS
- T_{motion} , transform matrix of the breathing and the patient motion in the world 3D CS, CS_w

$T_{\text{detector} \leftarrow w}$ and T_{proj} are assumed to be known for the X-ray images because of the known geometry and orientation of the C-arm. $T_{w \leftarrow 3\text{DRA}}$ is the identity because the 3D acquisition is around the iso-center of the C-arm. T_{motion} will be the result of our registration.

It then follows that a 3D point in the 3DRA, $p_{CS_{3\text{DRA}}}$, can be projected on CS_{fluoro} using the following equation (in homogeneous coordinates):

$$p_{CS_{\text{fluoro}}} = T_{\text{proj}} \cdot T_{\text{detector} \leftarrow w} \cdot T_{\text{motion}} \cdot T_{w \leftarrow 3\text{DRA}} \cdot p_{CS_{3\text{DRA}}} \quad (1)$$

The catheter is defined as an ordered set of N points:

$$C_{2\text{D}} = \{c_1, c_2, \dots, c_i, \dots, c_N\}$$

where $c_i \in \mathbb{R}^2$ is a 2D point at the center of the catheter in CS_{fluoro} . Note that c_1 is the tip of the catheter.

The blood vessel tree extracted from 3DRA is represented as a directed tree:

$$G_{3\text{D}} = (V, E)$$

where V is the set of 3D points of the centerlines in $CS_{3\text{DRA}}$ and E the set of directed edges between points.

2.2 Vessel selection based on shape similarity

Given the complexity of the blood vessel tree, we first select the most likely matching vessels for registration. To achieve this, we rank all possible vessels of $G_{3\text{D}}$. One vessel is a set of points starting from any location in the tree $G_{3\text{D}}$ to its root. The ranking is based on shape similarity between the 2D catheter and the 2D projection of the 3D blood vessel path; we use the following metric for the shape similarity S :

$$S = \int_0^l \vec{C}_{2\text{D}}(u) \cdot \vec{f}(S_{3\text{D}}(u)) du \quad (2)$$

where l is the length of the 2D catheter, $S_{3\text{D}}$ is one vessel from $G_{3\text{D}}$ and f is the 2D projection $f = T_{\text{proj}} \cdot T_{\text{detector} \leftarrow w} \cdot T_{w \leftarrow 3\text{DRA}}$.

This shape similarity metric integrates the ‘alignment’ of both structures (based on the dot-product of their direction vectors). The resulting value is in the range $[0, 1]$, and a high value implies a good match. This metric is not robust to large rotational motions, as those will change the orientation. As we are focusing on correcting for breathing motion, we expect the rotational motion to be small, and thus this metric should be sufficient. After computing the shape similarity for all possible vessels, the K best ranking vessels are used in the subsequent registration.

2.3 Rigid 2D/3D registration with forward projection

To match the 2D catheter with the vessels, we need to find the rigid transform T_{motion} in CS_w that yields the best match with the 2D catheter in CS_{fluoro} . We decompose the transformation as follows:

$$T_{\text{motion}} = T_{w \leftarrow \text{detector}} \cdot T_{\text{translation}} \cdot T_{\text{detector} \leftarrow w} \cdot T_{\text{rotation}}$$

where T_{rotation} is a rotation matrix with three unknowns (Euler angles, α , β and γ) and $T_{\text{translation}}$ is a translation matrix with three unknowns (x , y , z), where the translations are aligned with CS_{detector} . A translation along the projection axis in CS_{detector} will only have a very minor effect in the projection. We therefore exclude z from the registration parameters, leaving us with a five degrees of freedom transformation.

The distance metric we use is based on the distances in CS_{fluoro} . It is the sum of the minimal distance between each point of the catheter and any point of the current 3D selected vessel:

$$Dist(c, S, t) = \min_{s \in S} \|c - f(s, t)\| \quad (3)$$

where $c \in \mathbb{R}^2$, S is a vessel, t is a rigid transformation matrix and $f(s, t) = T_{\text{proj}} \cdot T_{\text{detector} \leftarrow w} \cdot t \cdot T_{w \leftarrow \text{3DRA}} \cdot s$.

The final transformation is the one with the smallest cumulative distance metric.

$$T_{\text{motion}} = \arg \min_{t \in T} \sum_{c \in C_{2D}} Dist(c, S_{3D}^{\text{sel}}, t) \quad (4)$$

where T is the set of possible rigid transformation matrices and S_{3D}^{sel} is one of the K best ranking selected vessels from G .

We apply a brute force search for the optimum over the five unknowns search space, which is feasible as the search space is small in case of breathing motion. The registration is performed among the K selected vessels and we keep the one with the smallest distance metric.

3 Experiments and Results

To evaluate the accuracy and the robustness of our method, we propose three experiments: one on phantom data, one with clinical data and the last one with clinical data and simulated catheter positions (therefore with a ground truth).

3.1 Parameters

We set the intervals of our brute force search to ± 50 mm (with 0.2 mm step) for x and y and $\pm 7^\circ$ (with 0.05° step) for α , β and γ . These intervals are sufficiently large to capture breathing motion. K is set to 5. The computation time is less than one minute for each frame.

3.2 Phantom acquisition

In the first experiment, we evaluate the method in the context of ideal data. To this end, we used two rigid phantoms (Fig. 3): a heart phantom with coronary arteries and one made of copper wire. We acquired 3DRA images of these phantoms and subsequently we acquired fluoroscopic images: 10 and 21 images for the heart and copper phantom, respectively. Each image has a different C-arm angle either in propeller or in roll positions. The intervention table and the phantoms were fixed, thus the relation between the 3DRA and the fluoroscopy is given by the positioning information of the C-arm system. Next, we registered the X-ray images to the 3DRA. In order to provide an impression of the registration accuracy, for each frame, the median of the remaining distances (Eq. 3) is presented in Fig. 3 : $Dist(c, S_{3D}^{best}, T_{motion})$ for each $c \in C_{2D}$ where S_{3D}^{best} is the best registered vessel from the K best ranking selected vessels. As we do not use calibrated angles of the C-arm, we observe an offset before the registration. The offset is much larger with the second phantom. This is caused by different C-arm motions (roll and propeller) during 3DRA and fluoroscopy acquisition.

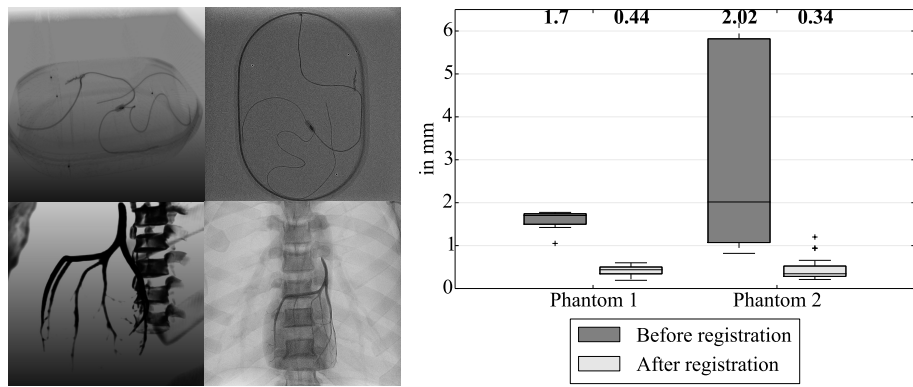


Fig. 3. (left) 3DRAs and fluoroscopies of both phantoms. (right) Medians of the distances between 2D catheter points and 2D projected 3D vessels points, for every segmented frames.

3.3 Clinical data

In the next experiment we evaluate the performance of the method with clinical data. To this end, we retrospectively acquired image data from 13 TACE procedures. For each TACE procedure, we have one 3DRA acquired during the inhalation phase when the catheter is in the left or right hepatic artery and several (from 1 to 15) X-ray sequences. In total, we acquired 101 X-ray sequences. In each sequence, we segmented the catheter manually in three frames: one in inhale, one in exhale and one in-between. We applied our registration approach

on each of these 303 frames, using the C-arm information and the initial position of the 3DRA. We report the median of the distances between the catheter points and the best vessel points (Eq. 3), and also visually inspected the results.

Figure 4 shows the results of the registration on clinical data. In all except two cases, the median of the distances, for each patient, is below 1 mm. In the case of one patient, the 3DRA image is of low quality, and parts of the vasculature are missing, especially the hepatic and aorta. For the other patient with a larger median distance, the 3DRA acquisition was not correctly centered on the liver, so part of the hepatic and aorta are not in the 3DRA. We obtained the following medians of the average of the distances (Eq. 3): 1.35 mm, 1.45 mm and 1.78 mm for 'inhale', 'in-between' and 'exhale', respectively. Unlike medians in Fig. 4, averages point out differences between the breathing states. The medians of the average of the distances close to the tip (10% of the catheter) are: 1.46 mm, 1.59 mm and 1.54 mm. When we visually checked the registrations, in 71% of the cases, the correct vessel was registered (Fig. 5). In the other cases, the registration was incorrect: 58% due to 3DRA misacquisition and 20% due to large catheter deformation.

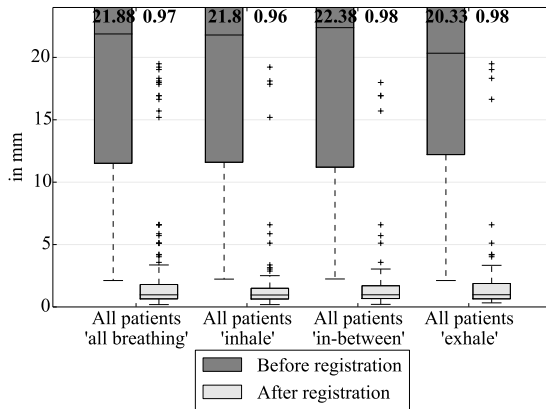


Fig. 4. Medians of the distances between 2D catheter points and 2D projected 3D vessels points, for every segmented frames

3.4 Clinical data with a simulated catheter

Finally, we used the same clinical images to generate synthetic data for which we have a ground truth. We used all clinically acquired 3DRAs, but instead of using fluoroscopies and a manually segmented catheter, we annotated an artificial catheter in the 3DRA vasculature (using the registered vessel from previous results of clinical data) and then project it as 2D curve onto the fluoroscopic image, using the C-arm settings. To achieve this, we used the set of frames

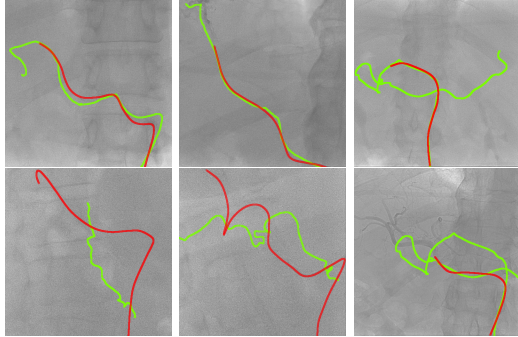


Fig. 5. Registration of the catheter (red) and the best registered vessel (green). (top) Successful registrations. (bottom) Missed registrations. (bottom-left) 3D arterial tree segmentation misses too many vessels (aorta and hepatic artery). (bottom-middle) 3D arterial tree misses the aorta. (bottom-right) The distance metric does not take into account the vessel continuity.

at inhale (101 images). Additionally, we simulated the stretching behaviour of the catheter by applying a Gaussian kernel smoothing on the 3D annotated catheter curve and we applied different random translations and rotations for the transformation T_{motion} . We performed three simulations (slight, moderate and large) of breathing and deformations (Table 1). Breathing is done along the axis y .

Table 1. Parameter randomizations of the simulations

	Slight	Moderate	Large
Translation x (in mm)	[-30, 30]	[-30, 30]	[-30, 30]
Translation y (in mm)	[-20, 20]	[-40, -20] \cup [20, 40]	[-50, -40] \cup [40, 50]
Translation z (in mm)	[-30, 30]	[-30, 30]	[-30, 30]
Rotation α, β, γ (in $^\circ$)	[-6, 6]	[-6, 6]	[-6, 6]
Catheter smoothing σ	[1, 5]	[5, 10]	[10, 15]

As we know the exact position of the catheter, we can compute the distance between the real 2D catheter position and the 2D catheter position obtained by applying the registration result T_{motion} , and for the tip as well. Figure 6 shows these distances. We also report whether the registered vessel contains the catheter (Table 2).

4 Discussion

We presented and evaluated a method that is able to maintain alignment of liver vascular roadmaps in the presence of patient breathing, using a vessel selection and rigid registration approach. We evaluated the method on phantom,

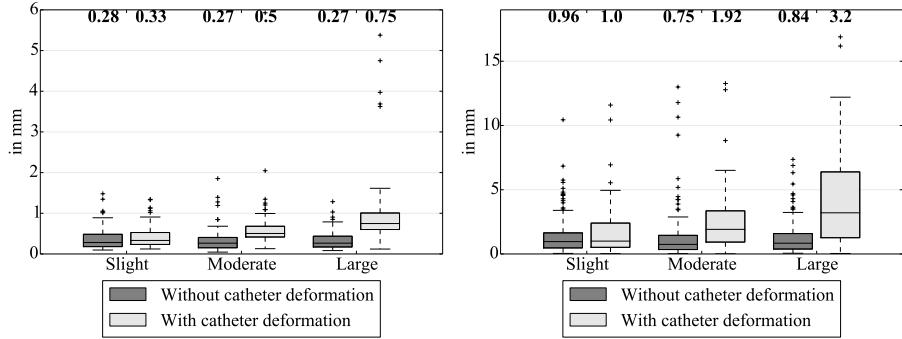


Fig. 6. (left) Medians of the distances between 2D catheter points and 2D projected 3D vessels points, for every segmented frames, after registration. (right) Distance between the real tip and the registered tip after registration.

Table 2. Percentage of tips inside the registered vessel

No catheter deformation			With catheter deformation		
Slight	Moderate	Large	Slight	Moderate	Large
88%	89%	92%	82%	89%	81%

clinical and simulated data. The median distances between catheter and vessel centerlines are below 1 mm for most cases. For the simulated data, the median of the tip position accuracy is below 2 mm, except when the catheter has a large deformation. Most of the registrations have small (< 1 mm) median distances, which demonstrates that the approach we propose is feasible. In addition, the third experiment, where the catheter does not exactly match the vasculature, demonstrated that the method is robust to deformations and relatively large displacements. However, the last experiment also demonstrated that a large deformation may lead to incorrect vessel selection. Furthermore, this experiment indicated that registration distance below 1 mm does not imply a tip position below 1 mm. Failure in accurate registration for the real patient data was often caused by insufficient quality (missing vessels) of the 3DRA data. This underlines the need of adequate imaging for our proposed approach.

Based on these results, we are considering several improvements. Firstly, adding temporal and contextual knowledge may reduce large misregistrations caused by incorrect vessel selections. Indeed, a catheter is more likely to be in the vessel that was used in previous registrations, especially in the case of slight catheter movement. Secondly, during the procedure, as the tip position is more important than the proximal part of the catheter, more weighting the registration result close to the tip may be relevant to improve the accuracy of the roadmap near the tip. Utilizing temporal information may also be beneficial here. Also, a real-time method should be achieved with advanced optimizers, the use of GPU and also by downsampling the catheter and blood vessel resolution. Lastly, in the future, we plan to investigate non-rigid registration as well, to

address those cases where the rigid registration fails to completely capture the breathing effects. It should yield better accuracy in case of deformation caused by catheter stiffness and breathing.

To conclude, we presented a method that allows performing continuous registration of a 3D vascular roadmap to 2D fluoroscopic images, based on the extracted vascular tree and the catheter position. We evaluated the feasibility of our approach on phantom, clinical and simulated data, demonstrating an overall median registration error less than 1 mm.

Acknowledgement. This research is funded by Philips Healthcare, Best, The Netherlands.

References

1. Groher, M., Zikic, D., Navab, N.: Deformable 2D-3D registration of vascular structures in a one view scenario. *IEEE Transactions on Medical Imaging* **28**(6) (June 2009) 847–860
2. Rivest-Henault, D., Sundar, H., Cheriet, M.: Nonrigid 2D/3D registration of coronary artery models with live fluoroscopy for guidance of cardiac interventions. *IEEE Transactions on Medical Imaging* **31**(8) (August 2012) 1557–1572
3. Jomier, J., Bullitt, E., Horn, M., Pathak, C., Aylward, S.R.: 3D/2D model-to-image registration applied to TIPS surgery. In: *Medical Image Computing and Computer-Assisted Intervention MICCAI 2006*. Volume 4191. Springer Berlin Heidelberg, Berlin, Heidelberg (2006) 662–669
4. Ma, Y., King, A., Gogin, N., Gijsbers, G., Rinaldi, C., Gill, J., Razavi, R., Rhode, K.: Clinical evaluation of respiratory motion compensation for anatomical roadmap guided cardiac electrophysiology procedures. *IEEE Transactions on Biomedical Engineering* **59**(1) (January 2012) 122–131
5. Metz, C., Schaap, M., Klein, S., Rijnbeek, P., Neefjes, L., Mollet, N., Schultz, C., Serruys, P., Niessen, W., van Walsum, T.: Alignment of 4d coronary cta with monoplane x-ray angiography. In: *Augmented Environments for Computer-Assisted Interventions*. Springer (2012) 106–116
6. Ruijters, D., Homan, R., Mielekamp, P., van de Haar, P., Babic, D.: Validation of 3d multimodality roadmapping in interventional neuroradiology. *Physics in Medicine and Biology* **56**(16) (2011) 5335–5354
7. Markelj, P., Tomažević, D., Likar, B., Pernuš, F.: A review of 3D/2D registration methods for image-guided interventions. *Medical Image Analysis* **16**(3) (April 2012) 642–661
8. Liao, R., Zhang, L., Sun, Y., Miao, S., Chef'd'hotel, C.: A review of recent advances in registration techniques applied to minimally invasive therapy. *IEEE Transactions on Multimedia* **15**(5) (August 2013) 983–1000
9. Atasoy, S., Groher, M., Zikic, D., Glocker, B., Waggershauser, T., Pfister, M., Navab, N.: Real-time respiratory motion tracking: roadmap correction for hepatic artery catheterizations. In: *Medical Imaging, International Society for Optics and Photonics* (2008) 691815–691815
10. Heibel, H., Glocker, B., Groher, M., Pfister, M., Navab, N.: Interventional tool tracking using discrete optimization. *IEEE Transactions on Medical Imaging* **32**(3) (2013) 544–555